Journal of Zhejiang University-SCIENCE A (Applied Physics & Engineering) in press
www.jzus.zju.edu.cn; www.springer.com/journal/11582
E-mail: jzus_a@zju.edu.cn

Research Article

https://doi.org/10.1631/jzus.A2300386

The preparation and properties of polyethylene glycol-*b*-poly (acrylamidophenylboronic acid) glucose responsive particles and their hyaluronic acid-based microneedle patches

Yichuan HONG[1], Haojie YU[1,2]✉, Li WANG[1,2], Xiang CHEN[1], Di SHEN[1], Yu WANG[1], Shuning REN[1], Yudi HUANG[1], Jian YANG[1]

[1]*State Key Laboratory of Chemical Engineering, College of Chemical and Biological Engineering, Zhejiang University, Hangzhou 310027, China*
[2]*Zhejiang-Russia Joint Laboratory of Photo-Electro-Magnetic Functional Materials, College of Chemical and Biological Engineering, Zhejiang University, Hangzhou 310058, China*

Abstract: To overcome the pain and risk of hypoglycemia in insulin administration, glucose-responsive microneedles have been developed by researchers, which could release insulin according to the blood glucose level. We designed a kind of particles by a RAFT method containing a phenylboronic acid group as the sensor of glucose and carrier of insulin. Polyethylene glycol (PEG)-DDMAT was synthesized as a macromolecular RAFT agent, which was then reacted with 3-acrylamidophenylboronic acid (AAPBA) to synthesize the block copolymer PEG-b-PAAPBA. Glucose-responsive particles loaded with insulin were prepared by self-assembly based on hydrophilic-hydrophobic interactions. Microneedle patches loaded with glucose-responsive particles were prepared using hyaluronic acid as the substrate. The insulin release behavior of the particles in glucose solutions of 0, 100, and 400 mg/dL showed significant glucose responsiveness and good biosafety. The results of blood glucose control experiments in rats indicate that a single microneedle patch can effectively maintain normal blood glucose for over 7 hours.

Key words: Diabetes; Hyaluronic acid; Phenylboronic acid; Glucose responsive hydrogel; Microneedles

1 Introduction

Diabetes is a chronic disease characterized by hyperglycemia, which can lead to metabolic syndrome, obesity, dyslipidemia, and hypertension, posing a threat to patients' health (Mayer-Davis et al., 2017). In 2021, there were 140 million diabetes patients in China (Chan et al., 2020). Insulin therapy is effective in relieving hyperglycemic symptoms in Type I and severe Type II diabetes. Microneedles are an efficient, convenient, and painless platform for transdermal insulin delivery (American Diabetes Association, 2018). Polymers containing phenylboronic acid (PBA) exhibit unique glucose-responsive properties under certain conditions. Glucose-responsive microneedles based on phenylboronic acid (PBA) groups can painlessly pierce the dermis and manage insulin release according to the blood glucose concentration (American Diabetes Association, 2018; Meng et al., 2020) to maintain a normal blood glucose level (Chen et al., 2020). Glucose-sensitive particles (NP) can be loaded into dissolving microneedles to obtain a kind of glucose-sensitive microneedle with a high insulin loading (Li et al., 2015). Using the reversible addition-fragmentation chain transfer (RAFT) method to synthesize polymers, followed by self-assembly, is an effective way to prepare glucose-responsive particles (Meng et al., 2020). Wu *et al*. (2017) synthesized a block copolymer, poly(3-acrylamidophenylboronic acid)-*b*-poly(methacrylic acid-*co*-ethylene glycol dimethyl ether methacrylate) by the RAFT method, which self-assembled into drug-loaded nanoparticles. The insulin loading capacity (LC) of the nanoparticles was about 15%, and the encapsulation efficiency (EE) was about 70%. Such particles need to form hydrophilic-hydrophobic structures to achieve responsiveness, making the preparation process more complicated (Wu et al., 2017). Polyethylene glycol (PEG) can be used to synthesize large molecular weight RAFT reagents, and then glucose-responsive block copolymers can be synthesized (Li et al., 2015). This type of polymer avoids complex reactions and has

✉ Haojie YU, hjyu@zju.edu.cn
Haojie YU, https://orcid.org/0000-0002-7405-7881

Received July 31, 2023; Revision accepted Oct. 17, 2023; Crosschecked

higher stability and lower cell toxicity, which is beneficial for reducing damage to cells and insulin (Li et al., 2015). Tong et al. (2018) prepared poly(ethylene glycol)-*b*-poly(3-acrylamidophenylboronic acid)-*b*-poly(4-(4,4,5,5-tetramethyl-1,3,2-dioxaborolan-2-yl)benzyl acrylate) to encapsulate insulin and glucose oxidase (GOx) for drug delivery to obtain drug-loaded particles. The particles exhibited good biocompatibility and water dispersibility, with a drug encapsulation efficiency of up to 87%. They demonstrated an insulin release behavior responsive to high blood glucose levels. The synthesis of a glucose-responsive block segment using 3-acrylamidophenylboronic acid (AAPBA) requires one step polymerization, reducing the synthetic difficulty (Senemoğlu et al., 2022). With a hydrophilic PEG chain and hydrophobic phenylboronic acid groups, block polymers can assemble into drug-loaded particles with hydrophilic-hydrophobic interaction

In this study, we used PEG and 2-(dodecylthio(thiocarbonyl)thio)-2-methylpropionic acid (DDMAT) to synthesize the macromolecular RAFT reagent PEG-DDMAT. PEG-*b*-AAPBA block polymer was prepared by the polymerization of the RAFT reagent and AAPBA monomer. Successful synthesis was proved by FTIR and ^{1}H NMR characterization. Afterward, glucose-sensitive particles were prepared by loading insulin with PEG-*b*-AAPBA through hydrophilic and hydrophobic interaction. The morphology was observed by SEM and TEM, and corresponding characterization was carried out by particle size and drug loading. The drug-loaded sugar-sensitive particles were then loaded into hyaluronic acid microneedles to achieve subcutaneous administration of insulin.

2 Materials and methods

2.1 Materials

HA (90-100 kDa) and cow insulin were purchased from Shanghai Yuanye Bio-Technology Co., Ltd. N-hydroxy succinimide (NHS, 98%), AAPBA (98%), mPEG (5000 Da), streptozotocin (STZ, 98%), 1-(3-dimethylaminopropyl)-3-ethylcarbodiimide hydrochloride (EDC, 97%) and 2,2'-azobis(2-methylpropionitrile)(AIBN) were purchased from Macklin Inc. PVA (Mowiol PVA-117, Mw: ~145000) and 4-dimethylaminopyridine (DMAP, 97%) were purchased from Shanghai Aladdin. Hydrochloric acid (HCl, AR), sodium hydroxide (NaOH, AR), N,N-dimethylformamide (DMF, AR), and ethylene diamine (AR) were purchased from Sinopharm. DDMAT (97%) was purchased from the Shanghai Bide Pharmaceutical Technology Co., Ltd.

2.2 Synthesis of macro RAFT agent PEG-DDMAT

Using the method of Senemoğlu et al. (2022), PEG-DDMAT was synthesized by EDCI/DMAP-catalyzed esterification reaction of PEG (5000 Da) with the DDMAT at 40 □. The preparation method was as follows: 4.6020 g (0.92 mmol) mPEG-5000, 0.5000 g (1.38 mmol) DDMAT, 0.5051 g (4.14 mmol) DMAP were dissolved in a 250-ml round-bottom flask in 60 ml CH_2Cl_2 (solution A). 396.4 mg (2.07 mmol) of EDCI was dissolved in 40 ml CH_2Cl_2 as solution B. Under the protection of Ar, solution B was slowly dropped into solution A through a dropping funnel while stirring at 500 rpm for 30 min, then the temperature was raised to 40 °C for 24 h. When the reaction was completed, the solvent was evaporated to about 25 mL and washed three times with 25 mL of saturated brine. The organic phase was washed three times with deionized water, then excess anhydrous $MgSO_4$ was added to the solution to remove water. The dispersion was filtered, then the filtrate was evaporated to about 25 mL and precipitated with 250 mL cold diethyl ether to obtain pale yellow products. The products were then dissolved again with 10 mL of CH_2Cl_2 and precipitated with 100 mL diethyl ether. 3.5482 g of pale-yellow products were obtained after drying, with a yield of around 71.7%.

2.3 Synthesis of PEG-*b*-PAAPBA

PEG-*b*-PAAPBA was obtained by RAFT polymerization (Zhou et al., 2016). Taking the sample PEG_{114}-*b*-$PAAPBA_{51}$ as an example: 0.2674 g (0.050 mmol) PEG-DDMAT, 0.4775 g (2.50 mmol) AAPBA, and 2.1 mg (0.025 mmol) AIBN were dissolved in a mixed solution of 9.5 ml DMF and 0.5 ml H_2O. After Ar bubbling treatment for 20 min, the reaction lasted for 12 h at 78 °C with stirring at 500 rpm and protection by Ar, and was stopped by cooling the system to room temperature. After the reaction, the solution was dialyzed (MWCO 3500) in 500 ml of DMF for one day. The dialysis bag was then dialyzed with 4 L deionized water for 5 days. The dialyzed

reaction solution was freeze-dried to constant weight to obtain 0.2156 g of product. Samples with monomer molar ratios of 1:25, 1:100, 1:200, 1:500, and 1:1000 were prepared according to the same method.

2.4 Preparation of polymer particles NP-PEG114-*b*-PAAPBA$_n$

The polymer particles were prepared according to the published method with minor adjustments (Wang et al., 2019). Taking NP-PEG$_{114}$-*b*-PAAPBA$_{51}$ as an example, 4.0 mg of PEG$_{114}$-*b*-PAAPBA$_{51}$ was dissolved in 400 μL pH=13 NaOH. This solution was rapidly added to PBS (10 mM, pH 7.4, 4.2 mL) with stirring at 800 rpm, and the pH was adjusted to 7.4 with 0.1 M HCl. After that, the dispersion was transferred into a 30-mL centrifuge tube and centrifuged at 12,000 rpm for 20 min. The supernatant was then removed. The precipitate was centrifuged and washed with deionized water according to the same parameters. The supernatant was removed and the precipitate was freeze-dried to obtain a powdery precipitate, which was designated NP-PEG$_{114}$-*b*-PAAPBA$_{51}$.

2.5 Preparation of drug-loaded particles ins-PEG114-*b*-AAPBA$_n$

When preparing drug-loaded particles, taking ins-PEG$_{114}$-*b*-PAAPBA$_{291}$ as an example, 4.0 mg of insulin and 4.0 mg of PEG$_{114}$-*b*-PAAPBA$_{291}$ were dissolved in 400 μL pH=13 NaOH, and then the dispersion was obtained by the same method as for the preparation of unloaded particles. After that, the dispersion was put in a centrifuge tube and centrifuged at 12,000 rpm for 20 min, then the supernatant was collected. The "Bradford" method was used to measure the insulin concentration (Yu et al., 2020). The sediment was washed once with 5 mL of deionized water according to the same parameters, then the supernatant was collected and the insulin concentration was measured again by the "Bradford" method to obtain the insulin content of the supernatant after washing (Yu et al. 2020; Shen et al., 2020). The precipitate obtained after freeze-drying was recorded as ins-PEG$_{114}$-*b*-PAAPBA$_{291}$. The encapsulation efficiency (EE) and drug loading (LC) were calculated from the sum of the serum insulin content (free insulin) and dry particle weight (NPs' weight) and the total insulin content (total insulin) using formulas (1) and (2):

$$\mathrm{EE\%} = \frac{\text{total insulin} - \text{free insulin}}{\text{total insulin}} \times 100\% \quad (1)$$

$$\mathrm{LC\%} = \frac{\text{total insulin} - \text{free insulin}}{\text{NPs' weight}} \times 100\% \quad (2)$$

2.6 *In vitro* insulin release from drug-loaded nanoparticles

Insulin release experiment: 1.5 mg of ins-PEG-*b*-PAAPBA was soaked in 4 mL of PBS solution containing 0, 100, or 400 mg/dL glucose, respectively. The solutions were incubated in a shaker at 37 °C for release. After each sample was centrifuged at 4000 rpm for 5 min, 200 μL of the supernatant was drawn for testing (Senemoğlu et al., 2022). After testing, 200 μL of PBS was injected into each tube.

Preparation of standard Coomassie brilliant blue solution: 100.3 mg (0.11 mmol) Coomassie brilliant blue G-250 was dissolved in 50 mL of ethanol, and 100 mL of 85% phosphoric acid was added to the solution. Then DI water was added until its volume reached 1 L.

Insulin standardization by Bradford assay: Firstly, the absorbance A_0 of the well plate was measured. Then 20 μL of insulin standard solution was taken to the plate, and 200 μL Coomassie blue solution was then then dropped into the wells for staining. A microplate reader was used to measure the absorbance A_{si0} at a wavelength of 595 nm. The actual absorbance A_{si}=A_{si0}-A_0. The actual absorbance of other insulin solutions was then measured in the same way. The absorbance-insulin concentration curve was then drawn with linear fitting (Yu et al., 2020).

Determination of insulin concentration by Bradford assay: The absorbance A_{i0} of the sample was measured using the same steps as when calibrating insulin, and the actual absorbance A_i= A_{i0}-A_0.

$$\text{Cumulative insulin release} = \sum_{n-1}^{i=1} 0.2(mL) \times c_i + 4(mL) \times c_n \quad (3)$$

Cumulative insulin release/mg refers to the total amount of insulin released from the gel during the test; c_n (mg/mL) refers to the concentration of the number n test.

2.7 Particle size characterization

The samples for particle size test were obtained by ultrasonically dispersing 0.5 mg/L of particle dispersion liquid for about 20 min. The particle size distribution was obtained using a Zetasizer Nano-ZS nanometer particle sizer with the temperature set to 25 ^{0}C. The average value of the three tests was taken.

2.8 TEM assay

TEM characterization was carried out using an HT-7700 120kV transmission electron microscope. Samples were prepared by dripping 10 μL of the dilute dispersion liquid onto the copper mesh covered with carbon film. The samples were observed after

drying.

2.9 SEM assay

SEM characterization was carried out using a scanning electron microscope SU-8010. Microneedles were observed after being sprayed with gold at 15 mA for 90 s. When observing the particles by SEM, a dilute solution of the particles was dispersed on a silicon wafer, followed by natural drying and spraying with gold.

2.10 NMR Characterization

Samples were tested by hydrogen nuclear magnetic resonance spectroscopy (^{1}H NMR) using a BRUKER ASCEND 500 nuclear magnetic resonance apparatus. DDMAT and PEG-DDMAT were characterized by dissolution in $CDCl_3$, and PEG-*b*-AAPBA was characterized by dissolution in D_2O containing 0.01 M NaOH.

2.11 Preparation of microneedle patches

The mold specifications of the microneedle patch for translation are 15×15 microneedle arrays, with a single needle height of 600 μm, a center-to-center distance of adjacent microneedles of 400 μm, and a bottom side length of 400 μm. The patch was purchased from the Micropoint Company. All particles loaded on the microneedles were ins-PEG_{114}-*b*-$PAAPBA_{291}$. During the vacuum preparation method, to ensure needle shape integrity and particle dispersibility, the tips of the microneedles were filled with a 5 wt% HA dispersion containing particles, while the base was filled with higher concentration of HA. The needles were coded. For example, MN-va-7.5%-1 represents a micro-needle prepared under vacuum conditions with a 7.5% concentration of HA in the base and loaded with 1.0 mg of particles (calculated as 0.35 mg insulin). To prepare MN-va-7.5%-1, 1.0 mg of drug-loaded particles (ins-PEG_{114}-*b*-$PAAPBA_{291}$) were dispersed in 50 μL of 5 wt% HA solution to obtain a particle dispersion liquid. The liquid was then used to fill the cavity of the mold at the tip of the micro-needle and maintained at 30 °C and 0.07 MPa vacuum for 2 h. Next, a 7.5 wt% HA solution was used to fill the base of the micro-needle, which was dried in a vacuum oven for 2 h to remove bubbles. After drying, the micro-needle patch was removed from the mold and coded MN-va-7.5%-1. When the particle loading capacity was increased to 2.0 mg, the micro-needle patch was coded MN-va-7.5%-2. The microneedle patch directly loaded with insulin was coded MN-va-ins. Changing the concentration of the HA solution used in the second injection molding to 5 wt% or 10 wt% produced microneedles coded MN-va-5%-1, MN-va-10%-1, etc.

The centrifugation method for preparing the micro-needle patch involved dispersing 1.0 mg of drug-loaded particles in 200 μL of 7.5 wt% HA and filling the mold cavity with about 150 μL. After centrifugation at 4000 rpm for 30 min, the mold was dried in a dryer for 1 day. The above steps were repeated for a second injection to obtain the micro-needle patch coded MN-ce-7.5%-1.

2.12 Characterization of mechanical properties of microneedles

The mechanical properties of the microneedles were characterized by mechanical compression and skin penetration. Mechanical compression was tested with a universal material tester (Zwick/Roell Z020). The microneedles were placed on the stage for compression with a compression distance of 500 μm and at a speed of 0.5 mm/s.

Skin penetration was tested using depilated mouse skin. The microneedle was pressed to penetrate the depilated rat skin, and pulled out after maintaining pressure for 3 min. Trypan blue solution (0.4%) was applied to the punctured area for staining. Successfully punctured holes turned blue, while unpunctured holes remained unchanged due to the presence of the stratum corneum on the surface. The mechanical properties of the microneedles were determined by the staining.

2.13 Hemolysis assay

Configuration of the sample extraction solution: taking the extraction solution of microneedles as an example, 8.0 mg of drug-loaded microneedles was cut. 0.01 M PBS solution at pH 7.4 was added to give a total mass of 8.0041 g and the microneedles were soaked at 37 °C for 2 h. The system was centrifuged at 1500 rpm for 10 min, then the supernatant was filtered with a 0.45-μm aqueous filter. The obtained filtrate was a 0.1-wt% extract of microneedles.

Configuration of red blood cell suspension: 5.0 mL of anticoagulated bovine blood was put into a centrifuge tube. 0.01 M pH 7.4 PBS was added to dilute to 25.0 mL. The suspension was centrifuged at 1500 rpm for 10 min, then the supernatant was removed. This was repeated 4-5 times until the supernatant clarified. 19 mL of PBS solution was then added to 1.0 mL of the clarified red blood cell dispersion to obtain a 5% volume fraction of red blood cell suspension for use.

Determination of hemolysis rate: To 0.2 mL of

red blood cell suspension, 0.8 mL of leaching solution (test group), PBS solution (negative control group), or deionized water (positive control group) were added, mixed, and kept at 37 ℃ for 2 h to obtain the culture medium. Then, the culture solution was placed in a centrifuge tube and centrifuged at 1500 rpm for 10 min. 200 μL of the supernatant was taken to measure the absorbance at a wavelength of 545 nm using a microplate reader. Each group of five parallel samples was used to calculate the hemolysis rate according to formula (4):

$$\text{Hemolysis rate}=\frac{(OD545_S-OD545_N)}{(OD545_P-OD545_N)}\times 100\% \quad (4)$$

2.14 Cytotoxicity assay

The 3-(4,5-dimethylthiazole-2)-2,5-diphenyltetrazolium bromide (MTT) colorimetric method was used to test cell viability after the reaction preparation process. 10.0-mg solid powder samples were sterilized under high pressure steam at 121 ℃ for 20 min. Then, 10 mL of complete medium was added to the sterilized samples and co-cultured at 37 ℃ for 24 h. The above mixture was centrifuged at 3500 rpm for 30 min, and the supernatant was taken as a 100% sample extract for later use. Afterwards, the leaching solution was diluted by volume to 25% (the sample group), 50% (the negative control group, high-density polyethylene leaching solution), 75% (the positive control group, DMSO containing 20 wt% PBS), or 100% (the blank control group, PBS).

Then, cell culture and absorbance detection experiments were carried out in accordance with the fifth part of GBT16886.5-2017 *in vitro* cytotoxicity experiments. L929 cells were cultured in 96-well plates for 24 h, and then 100 μL/well of leaching solution was added for culture. After the cells were seeded and cultured for 24 h, the medium was removed. Then, 100 μL of medium containing 0.5 mg/mL MTT was added to each well and cultured for 4 h. The supernatant was removed and 100 μL of DMSO added to each well. After shaking for 10 min, the absorbance at 570 nm was detected to determine the concentration of formazan in each well. The percent growth inhibition was calculated for each concentration tested.

2.15 *In vivo* insulin release assay

The experimental SD rats were provided by the Zhejiang Provincial Experimental Animal Center. The animal experiments were approved by the Zhejiang Provincial Experimental Animal Center Ethics Committee (approval number ZJCLA-IACUC-20010061). *In vivo* experiments were conducted by applying prepared microneedle patches to the STZ-induced type 1 diabetic SD rat model. The effect of insulin microneedle patches on blood glucose control was evaluated by measuring changes in rat blood glucose concentration over time (Shen et al., 2020).

The diabetes rat model was induced by injecting STZ solution. Firstly, 100 mg STZ was dissolved in 10 mL citric acid sodium citrate buffer. Secondly, the solution was injected into the peritoneal cavity of SD rats (average weight 220 g) at a dose of 110 mg STZ/kg body weight. After normal feeding for three days, the rats' weights and blood glucose concentrations were monitored and recorded. *In vivo* experiments were conducted when each rat's weight stabilized at 200 g and its blood glucose remained above 22 mmol/L (equivalent to 400 mg/dL) (Chen et al., 2021).

For the rat blood glucose control experiment, the same batch of SD rats was divided into six groups: Health group (blank group, no special treatment), SC group (subcutaneous injection of insulin group, 0.088 IU insulin/g rat body weight), MN-va-7.5%-1 group (microneedle patch prepared by vacuum method, 0.044 IU insulin/g rat body weight), MN-va-7.5%-2 group (microneedle patch prepared by vacuum method, 0.088 IU insulin insulin/g rat body weight), MN-va-ins group (directly loaded insulin microneedle patch prepared by vacuum method, 0.088 IU insulin/g rat body weight), and PBS group (subcutaneous injection of 0.01M pH=7.4 PBS solution with the same volume as the SC group). After fasting for 1 h (time zero), blood glucose was measured by taking blood from the rat's tail using a blood glucose meter (SinoCare Sinocare Stable+, Sinocare Biosensor Inc., Changsha, China). After 3 h, the rats were anesthetized. Then, successively the hair on the test area of the rats was removed using a razor and hair removal cream. The SC group was subcutaneously injected with insulin, while each microneedle group underwent microneedle patch attachment and fixation with 3M wound dressing tape. Afterward, the rats continued to be fasted (but allowed to drink water freely) and blood glucose was measured from the tail every hour until 11 hours or death. After the test was completed, the microneedle patches were removed, and the wound was stained with 0.4% trypan blue solution to record the staining situation.

3 Results and discussion

3.1 Synthesis of PEG-DDMAT

Figure 1 shows the synthesis reaction of macromolecular RAFT reagent PEG-DDMAT. The PEG part is monomethoxy-terminated mPEG, and PEG-DDMAT is synthesized by an esterification reaction catalyzed by EDCI/DMAP.

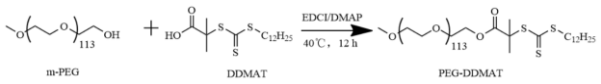

Fig. 1 Synthesis reaction of PEG-DDMAT

The synthesized PEG-DDMAT was characterized by FTIR (Zhou et al., 2016). The results are shown in Fig. 2. The characteristic peak corresponding to the polymer can be found in the FTIR spectrum. The broad peak near 3440 cm-1 corresponds to the stretching vibration peak of -OH, the peak at 1724 cm-1 corresponds to the characteristic peak of the stretching vibration of -C=O in the corresponding ester bond, and the peak at 1066 cm-1 corresponds to the characteristic peak of -C=S in the DDMAT part, and the corresponding O-CH_2-CH_2 signal peak at 1127 cm^{-1} belongs to the PEG part repeating unit (Senemoğlu et al., 2022), indicating that PEG-DDMAT was successfully synthesized after the reaction.

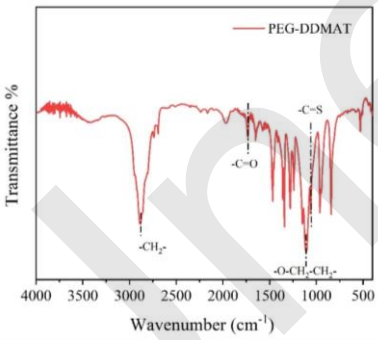

Fig. 2 FTIR spectrum of PEG-DDMAT

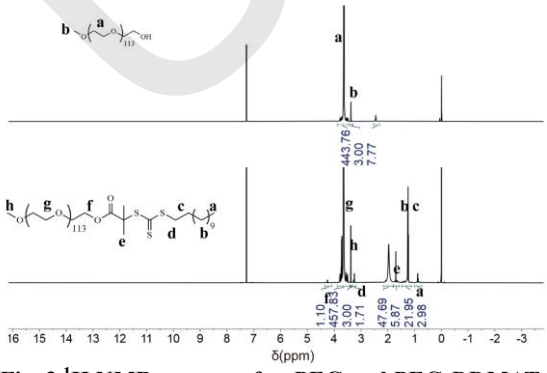

Fig. 3 ^{1}H NMR spectra of m-PEG and PEG-DDMAT

The structure of the product was characterized by ^{1}H NMR (Zhou et al., 2016) (Fig. 3). The peak at δ0.9 ppm in the spectrum is attributed to the methyl proton (a: 3H) of DDMAT, The peak at δ1.2-1.3 ppm corresponds to the methylene proton (b: 18H) in the DDMAT part. The characteristic peak near δ3.70 ppm corresponds to the proton (g: 4m-2 H) of the PEG repetitive single peak (-OCH_2CH_2-)$_m$, and the δ 3.45 ppm peak belongs to the methoxy-terminated proton of PEG (h: 3H). The successful synthesis of PEG-DDMAT was further demonstrated by the nuclear magnetic resonance hydrogen spectrum. According to formula (5), the number of repeat units of PEG was calculated by the areas Sg and Sa of peaks g and a, respectively.

$$m = \frac{S_g}{S_a} \times \frac{3}{4} \tag{5}$$

3.2 Synthesis of PEG_{114}-*b*-$PAAPBA_n$

The block copolymer PEG_{114}-*b*-$PAAPBA_n$ was synthesized by the macromolecular RAFT reagent PEG-DDMAT. The addition of experimental materials is shown in Table 1, and the reaction formula in Fig. 3. The reaction was initiated by AIBN, and then the block copolymer PEG_{114}-*b*-$PAAPBA_n$ was obtained by chain transfer of the RAFT reagent. Due to the large molecular weight of PEG and the steric effect, the number of monomers polymerized is relatively small. PEG-DDMAT and AAPBA were put into the reactor for reaction according to the molar ratio of 1:25 to 1:1000. The final product nuclear magnetic resonance hydrogen spectrum is shown in Fig. 5 (Zhou et al., 2016). The multiple peaks at δ 0.9-2.78 ppm are attributed to the protons in the alkyl chain of DDMAT (e: 25H) and the main chain protons in the block part of PAAPBA (d: 3n H). The peak at δ 1.2-1.3 ppm corresponds to the methylene proton (b: 18 H) in the DDMAT fraction. The δ 3.40 ppm peak corresponds to the methoxy group terminated proton (a: 3 H) of PEG. The multiple peaks at δ 6.75-7.80 ppm are attributed to the proton (c: 4n H) on the benzene ring of the AAPBA block. According to the nuclear magnetic resonance hydrogen spectrum (Fig. 6), the number of repeat units n of AAPBA can be calculated from the peak area S_c and the peak area S_b of c according to formula (6). The final products are PEG_{114}-*b*-$PAAPBA_{11}$, PEG_{114}-*b*-$PAAPBA_{51}$, PEG_{114}-*b*-$PAAPBA_{117}$, PEG_{114}-*b*-$PAAPBA_{291}$, PEG_{114}-*b*-$PAAPBA_{324}$, PEG_{114}-*b*-$PAAPBA_{441}$ and PEG_{114}-*b*-$PAAPBA_{954}$.

Table 1 Synthesis of PEG_{114}-b-$AAPBA_n$

Sample	PEG-DDMAT (d)		AAPBA (a)		AIBN		DMF	H_2O	d:a
	g	mmol	g	mmol	mg	mmol	ml	ml	
PEG_{114}-*b*-$AAPBA_{11}$	0.2679	0.050	0.2386	1.25	4.1	0.025	9.5	0.5	25
PEG_{114}-*b*-$AAPBA_{51}$	0.2674	0.050	0.4775	2.50	2.1	0.012	9.5	0.5	50
PEG_{114}-*b*-$AAPBA_{117}$	0.1337	0.025	0.4780	2.50	1.1	0.006	9.5	0.5	100
PEG_{114}-*b*-$AAPBA_{291}$	0.0668	0.013	0.4769	2.50	1.0	0.005	9.5	0.5	200
PEG_{114}-*b*-$AAPBA_{324}$	0.0131	0.025	0.2390	1.25	2.4	0.013	9.5	0.5	500
PEG_{114}-*b*-$AAPBA_{954}$	0.0126	0.025	0.4751	2.49	2.4	0.013	9.5	0.5	1000

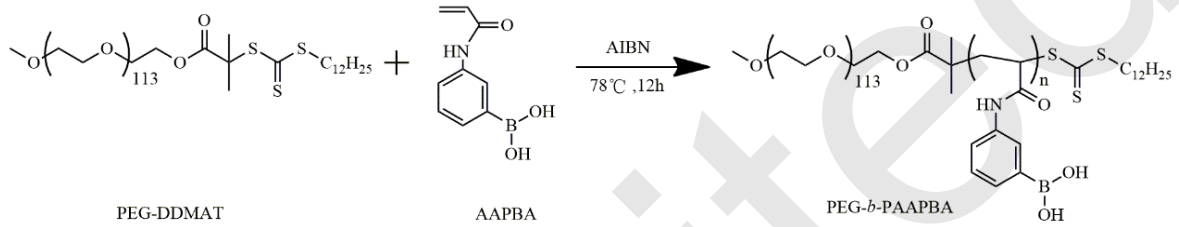

Fig. 4 Synthesis of PEG-*b*-AAPBA

Table 2 Polymer particle size of NP-PEG_{114}-*b*-$PAAPBA_n$

Sample	PEG_{114}-*b*-$AAPBA_n$		H_2O (ml)	Time (h)	pH	D_h
	mg	mmol				
NP-PEG_{114}-*b*-$AAPBA_{117}$	5.1	2.2×10^{-4}	10	1	7.4	663
NP-PEG_{114}-*b*-$AAPBA_{291}$	5.0	1.0×10^{-4}	10	1	7.4	487
NP-PEG_{114}-*b*-$AAPBA_{324}$	5.1	0.8×10^{-4}	10	1	7.4	415
NP-PEG_{114}-*b*-$AAPBA_{954}$	5.1	0.3×10^{-4}	10	1	7.4	239

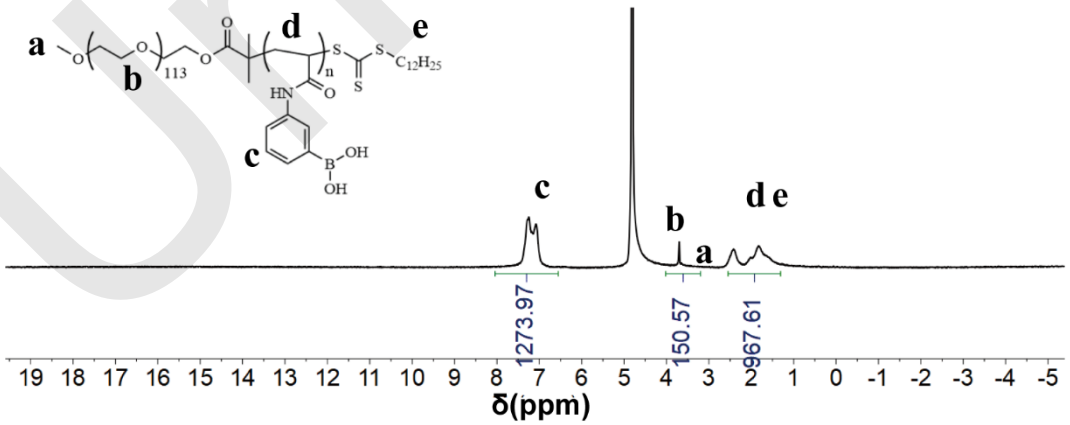

Fig. 5 ^{1}H NMR spectrum of PEG_{114}-*b*-$PAAPBA_{954}$

$$n = \frac{S_c}{S_b} \times 113 \quad (6)$$

3.3 Preparation and characterization of NP-PEG-*b*-PAAPBA particles

Under alkaline conditions, insulin and PEG-*b*-PAAPBA can dissolve in water, but their sol-

ubility decreases significantly under neutral conditions (Wang et al., 2019). Therefore, by dissolving the polymer in an alkaline solution and rapidly adding the system into a neutral or acidic solution, PEG-*b*-PAAPBA with hydrophilic-hydrophobic structures can self-assemble into NP-PEG-*b*-PAAPBA particles, or co-precipitate with insulin to produce ins-PEG-*b*-PAAPBA particles (Fig. 7). The particle size of the prepared particles was measured and the particle size distribution is shown in Table 2. The content of hydrophobic PBA group increases, the particles formed a denser hydrophobic core, and the particle size decreased from 1189 nm to 239 nm. SEM was used to further observe the particle morphology (Fig. 8). NP-PEG$_{114}$-*b*- PAAPBA$_{117}$ exhibited a large proportion of particles with diameters less than 100 nm and a few uniform particles with diameters in the hundreds of nanometers. The particles of NP-PEG$_{114}$-*b*-PAAPBA$_{291}$ and NP-PEG$_{114}$-*b*-PAAPBA$_{324}$ were mostly homogeneous and spherical with a relatively uniform size distribution, consistent with the results of particle size distribution testing. However, NP-PEG$_{114}$-*b*-PAAPBA$_{954}$ particles showed more obvious agglomeration, appearing as particle powder.

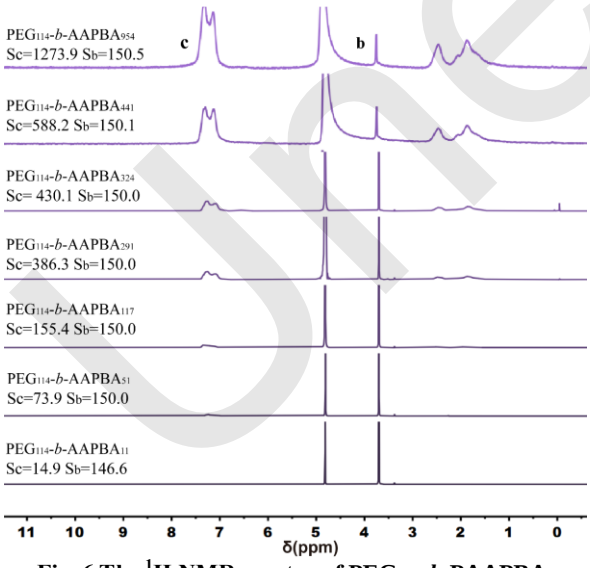

Fig. 6 The ^{1}H NMR spectra of PEG$_{114}$-*b*-PAAPBA$_n$

To determine the optimal pH value for particle preparation, the relationship between pH and particle size was investigated. Optical images and the specific particle size distribution are shown in Figs. 9 and 10, respectively. After one day of particle formation, at pH 6 the particles had completely precipitated, at pH 11 they no longer showed an obvious suspension state, and between pH 7 and pH 10 they had dispersed as particles. However, the stability of the particles to pH was insufficient at this time, and there were obvious changes in particle size under pH changes. The dispersity coefficient PDI was maximum at pH 9, but the particles may have had an insufficient encapsulation rate and insulin leakage. Therefore, it is necessary to reduce the pH appropriately to balance the stability and responsiveness of the particles. Considering that the pH value of the human body is about 7.4, the particles were prepared under conditions of pH 7.4.

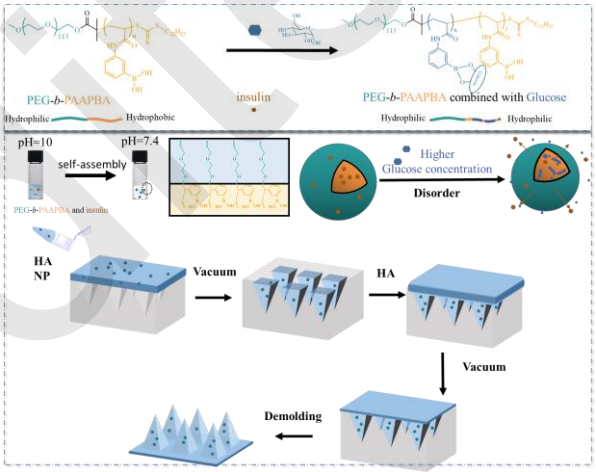

Fig. 7 Preparation of NP-PEG$_{114}$-*b*-PAAPBA$_n$ and the MN patch

3.4 Preparation of insulin-loaded particles ins-PEG$_{114}$-*b*-PAAPBA$_n$

Insulin and PEG-*b*-PAAPBA dissolved in water under alkaline conditions, but under neutral conditions the hydrophobicity of the PAAPBA segment in the polymer and insulin would increase (Wang et al., 2019). Therefore, when the solution pH shifted from alkaline to neutral, insulin and PEG-*b*-PAAPBA co-precipitated to form particles for loading. The results of the loading are shown in Table 3. As the length of the hydrophobic segments increased, both the drug-loading capacity and the encapsulation efficiency of insulin improved. The drug-loading capacity increased from 30.3% to 45.2%, and the encapsulation efficiency from 43.5% to 82.8%. These observations suggest that longer AAPBA segments are

more conducive to insulin loading. The morphology of the particles was observed. Figure 11 shows the SEM image of ins-PEG$_{114}$-*b*-PAAPBA$_{291}$ particles, which were spherical with a diameter of about 400-500 nm, consistent with the results obtained by light scattering. Further characterization of the particle morphology was performed using TEM (Fig. 12). The particles had a diameter of about 500 nm, and after treatment for 1 h at 100 mg/dL, they became vesicular, with some relative shrinkage and partial rupture of the particle diameter, indicating that the particles had some responsiveness to glucose.

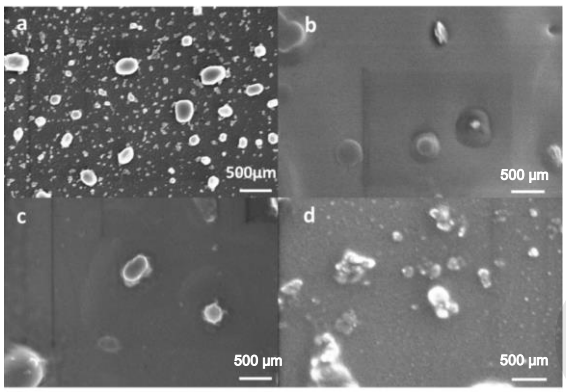

Fig. 8 SEM images of particles a: NP-PEG$_{114}$-*b*-PAAPBA$_{117}$, b: NP-PEG$_{114}$-*b*-PAAPBA$_{291}$, c: NP-PEG$_{114}$-*b*-PAAPBA$_{324}$, d: NP-PEG$_{114}$-*b*-PAAPBA$_{954}$ (pH=7.4)

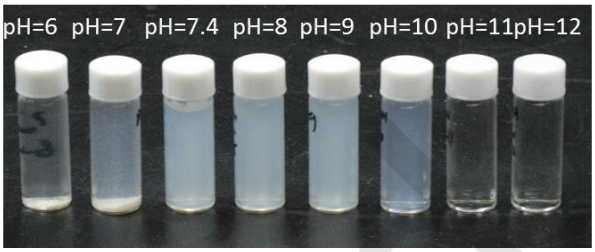

Fig. 9 Image of NP-PEG$_{114}$-*b*-AAPBA$_{291}$ particles under different concentrations of glucose

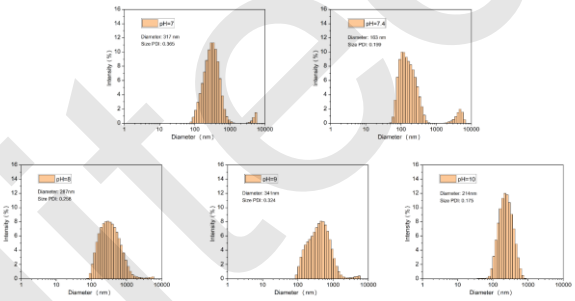

Fig. 10 Size distributions of NP-PEG$_{114}$-b-AAPBA$_{291}$ particles at different pH levels

Table 3 Insulin loading and encapsulation efficiency of ins-PEG$_{114}$-*b*-PAAPBA$_n$

Sample	PEG$_{114}$-*b*-PAAPBA$_n$		insulin	PBS	pH	LC%	EE%
	mg	$\times10^{-4}$mmol	(mg)	(mL)			
ins-PEG$_{114}$-*b*-PAAPBA$_{117}$	4.1	2.3	4.0	5.0	7.4	30.3	43.5
ins-PEG$_{114}$-*b*-PAAPBA$_{291}$	4.0	1.0	4.1	5.0	7.4	34.8	61.2
ins-PEG$_{114}$-*b*-PAAPBA$_{324}$	4.1	0.7	4.0	5.0	7.4	40.2	67.1
ins-PEG$_{114}$-*b*-PAAPBA$_{954}$	4.1	0.2	4.0	5.0	7.4	45.2	82.8

3.5 Glucose-responsive behavior of particles

The glucose-responsive properties of the particles were characterized by analyzing their size at different sugar concentrations. Taking NP-PEG$_{114}$-*b*-PAAPBA$_{291}$ particles as an example, the change in particle size after treatment with different concentrations of glucose for 1 h was investigated (Table 4). The particle size distribution results are shown in Fig. 13, with a hydraulic diameter (D_h) of 241 nm at a sugar concentration of 0 mg/dL, 233 nm at 100 mg/dL, and 215 nm at 400 mg/dL. As the sugar concentration increased, the particle size decreased, either by squeezing out insulin or by partial disintegration of the particles. With increasing treat-

ment time, the particles disintegrated further and released insulin. The release of insulin from the particles in response to glucose was evaluated using an *in vitro* insulin release experiment (Yu et al., 2020). The particles were immersed in PBS solutions with glucose concentrations of 0, 100, and 400 mg/dL to simulate the human environment, and the release experiment was conducted at 37 °C and pH 7.4 (Shen et al., 2020). All four types of particles exhibited glucose-responsive behavior in the release of insulin, with higher sugar concentrations resulting in higher release rates and amounts of insulin (Fig. 14). For example, in the case of ins-PEG_{114}-*b*-$PAAPBA_{291}$ at 0, 100, and 400 mg/dL glucose concentrations, the particles released 0.22 mg, 0.32 mg, and 0.46 mg of loaded insulin, respectively, within 7 h. With an increase in PBA content, insulin release in response to glucose became more pronounced, but the total amount released decreased. For example, under high sugar (400 mg/dL) conditions, ins-PEG_{114}-*b*-$PAAPBA_{117}$ released 0.52 mg of insulin, ins-PEG_{114}-*b*-$PAAPBA_{291}$ released 0.46 mg, ins-PEG_{114}-*b*-$PAAPBA_{324}$ released 0.41 mg, and ins-PEG_{114}-*b*-$PAAPBA_{954}$ released 0.42 mg. The insulin release of ins-PEG_{114}-b-$PAAPBA_{117}$ at glucose concentrations of 100 mg/dL and 400 mg/dL did not show a significant difference, but ins-PEG_{114}-*b*-$PAAPBA_{291}$ showed a relatively significant glucose-responsive release ability with a higher insulin release. Therefore, ins-PEG_{114}-*b*-$PAAPBA_{291}$ was used to fill the microneedles for subsequent microneedle performance experiments.

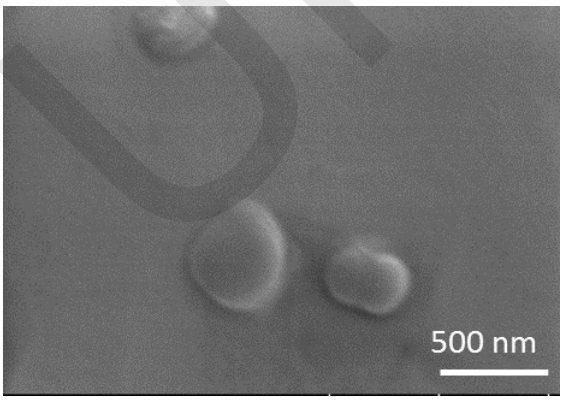

Fig. 11 SEM image of Ins-PEG_{114}-*b*-$AAPBA_{291}$ particles

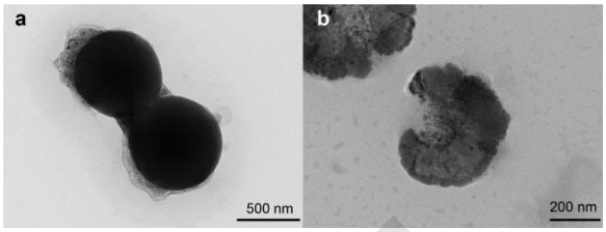

Fig. 12 TEM images of ins-PEG_{114}-*b*-$PAAPBA_{291}$ particles under (a) 0 mg/dL and (b) 100 mg/dL glucose concentration (pH=7.4, t=1 h)

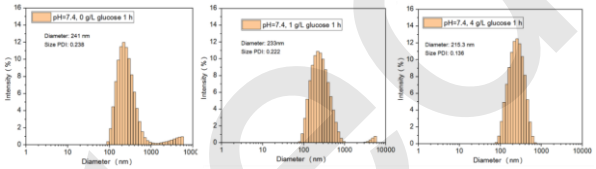

Fig. 13 Size distribution of PEG_{114}-*b*-$AAPBA_{291}$ particles under different concentrations of glucose

Table 4 Particle size distribution of PEG_{114}-*b*-$PAAPBA_{291}$ particles under different glucose concentrations

Sample	PEG_{114}-*b*-$PAAPBA_{291}$		Glucose		H_2O	Time	pH	Dh
	mg	mmol	mg	mmol	mL	h		nm
1	5.1	0.0004	0	0	10.0	1	7.4	241
2	5.0	0.0004	5.1	0.03	10.0	1	7.4	233
3	5.1	0.0004	20.6	0.11	10.0	1	7.4	215

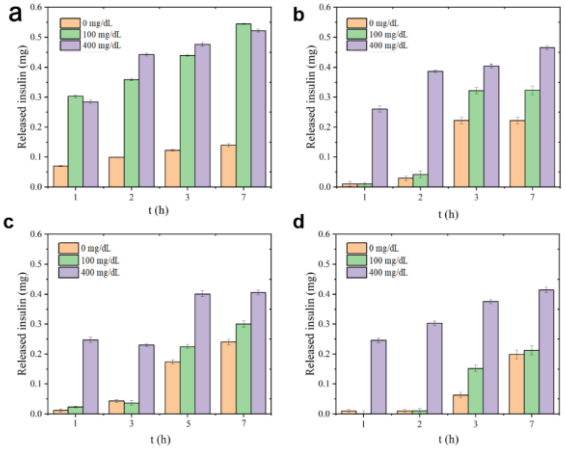

Fig. 14 *In vitro* insulin release of drug-loaded particles: (a) ins-PEG_{114}-*b*-$PAAPBA_{117}$, (b) ins-PEG_{114}-*b*-$PAAPBA_{291}$, (c) ins-PEG_{114}-*b*-$PAAPBA_{324}$, (d) ins-PEG_{114}-*b*-$PAAPBA_{954}$

3.6 Preparation and characterization of microneedle patches

Microneedle patches were prepared using HA as the matrix, with preparation parameters shown in Table 5. Patches were prepared by vacuum or centrifugation methods, and were loaded with particles containing unequal amounts of encapsulated insulin. Figure 15 shows microneedle patches prepared under different vacuum conditions at room temperature. Too low a vacuum (0.05 MPa) led to incomplete filling of the microneedles, while too high a vacuum (0.09 MPa) caused large bubbles to form at the end of the microneedles and on the substrate, resulting in poor uniformity. Therefore, a vacuum pressure of about 0.07 MPa was used for subsequent preparation. The morphology of the obtained microneedle patches was observed by SEM. Regardless of whether they were prepared by centrifugation or vacuum methods, the shaping rate of the microneedles was close to 100% and they exhibited a clear pyramid shape (Fig. 16). The height of a single microneedle of patch MN-va-7.5% prepared by the vacuum method was between 400 and 450 μm. This was slightly shorter than that of MN-ce-7.5% prepared by the centrifugation method at between 450 and 500 μm, but its height was still sufficient to penetrate into the dermis and achieve drug delivery. The mechanical properties of the microneedle patches were characterized by carrying out compressive experiments on a series of microneedle patches prepared by the various methods (Table 5).

Table 5 Preparation of microneedles

Sample	HA solution (per patch)		Insulin (per patch)		Vaccum time (0.07MPa) (min)	Centrifugal time (min)
	mg	wt%	mg	UI		
MN-ce-10%	100	10	0	0	0	45
MN-ce-10%-1	100	10	0.5	14	0	45
MN-ce-10%-2	100	10	1.0	28	0	45
MN-va-10%-1	100	10	0.5	14	120	0
MN-va-10%	100	10	0	0	120	0
MN-va-5%	100	5	0	0	120	0
MN-va-7.5%	100	7.5	0	0	120	0
MN-va-7.5%-1	100	7.5	0.5	14	120	0
MN-va-7.5%-2	100	7.5	1.0	28	120	0

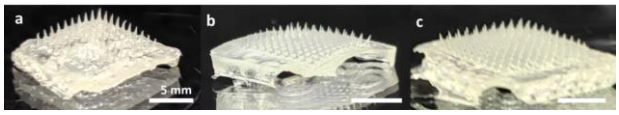

Fig. 15 MN prepared under different degrees of vacuum (at 30 °C): (a) 0.05 MPa, (b) 0.07 MPa, (c) 0.09 Mpa

The mechanical properties of microneedle patches were characterized through compression experiments. The mechanical strength of micro-needles fabricated by the vacuum method increased with increasing HA content when the substrate was prepared from 5 wt% or 7.5 wt% HA (Fig. 17). Its modulus was slightly higher than MN-ce-10%. However, when the HA content was increased to 10%, the mechanical properties decreased significantly due to the high viscosity of the solution and the low rate of microneedle formation. Because the vacuum method is beneficial for batch preparation of microneedle patches and MN-va-7.5% had the highest compressive modulus, MN-va-7.5% was used to prepare the microneedle patches in subsequent experiments. Figure 17b shows that as more insulin particles were loaded on the microneedle patch, the mechanical properties deteriorated. At a compression distance of 300 μm, the single needle puncture forces of MN-va-7.5%, MN-va-7.5%-1, and MN-va-7.5%-2 were 0.022 N, 0.017 N, and 0.015 N, respectively. In the puncture experiment, the strength of microneedles was characterized by sealing film and rat skin puncture experiments (Fig. 18). In the puncture experiment of the sealing film, the thickness of a single layer of Parafilm M was 127 μm. The microneedle could puncture two layers of sealing film to obtain a puncture array after being withdrawn. The puncture rate was obtained by dividing the number of puncture holes on the array by the number of microneedles. The puncture rate of MN-va-7.5%-1 was about 100%, and the puncture rate of MN-va-7.5%-2 was close to 60%. Therefore, for animal epidermal layers with both mechanical strength and thickness less than the sealing film, microneedle patches should effectively penetrate the epidermal layer and enter the dermis layer. Rat skin puncture experiments were then performed using microneedle patches, and the skin wound array was stained with trypan blue. The puncture rates of microneedles on each group of rat skin were between 80% and 100%.

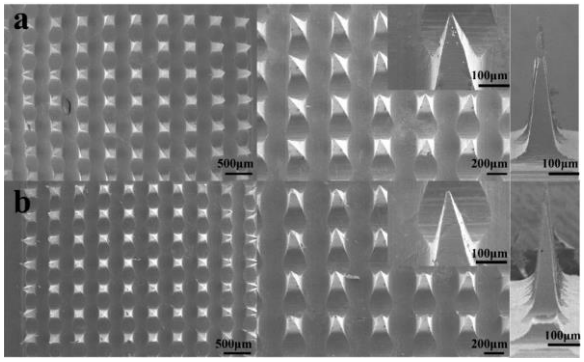

Fig. 16 SEM images of MN patches: (a) MN-va-7.5%, (b) MN-ce-7.5%

3.7 Cell toxicity and hemolysis experiments of microneedle patches

L929 cells were cultured for 24 h in various sample extracts containing medium, and the cell toxicity of each sample group was evaluated based on their proliferation (Yu et al., 2020). Figure 19 shows the MTT test results of microneedle patches and particles. The cell activity in each culture medium was close to 100%, indicating excellent cell compatibility. The hemolysis test results are shown in Fig. 20.

The hemolysis rates of NP-PEG$_{114}$-*b*-PAAPBA$_{291}$ and NP-PEG$_{114}$-*b*-PAAPBA$_{324}$ were both less than 5%, showing low red blood cell lysis (Yu et al., 2020), when water was used as the anode positive control group (hemolysis rate 100%) and 0.01 M PBS was used as the negative control group (hemolysis rate 0%). The hemolysis rate of NP-PEG$_{114}$-*b*-PAAPBA$_{117}$ was slightly higher than 5%, which may be due to its partial dissolution in PBS solution.

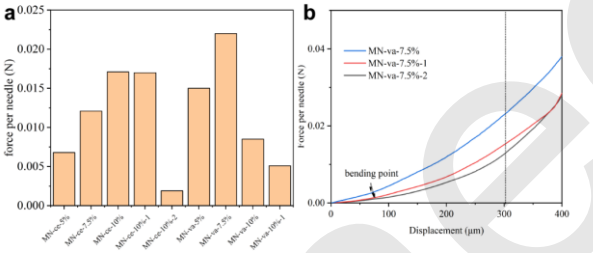

Fig. 17 a: Compressive strength of MNs (compression distance 300 μm), b: Compressive strength of MN-va-7.5%, MN-va-7.5%-1, MN-va-7.5%-2

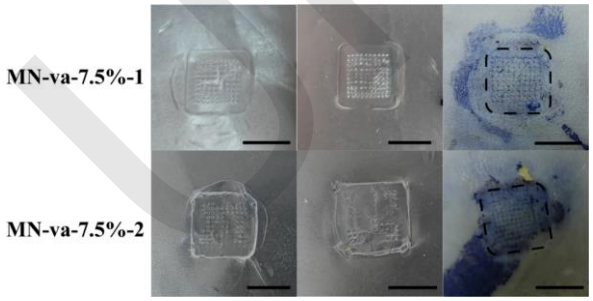

Fig. 18 MN piercing experiment images: Sealing film with a thickness of 127 μm was punctured with a microneedle patch. The mouse skin was punctured with a microneedle patch and the wound area was stained with 0.4% trypan blue solution (scale bar 5 mm)

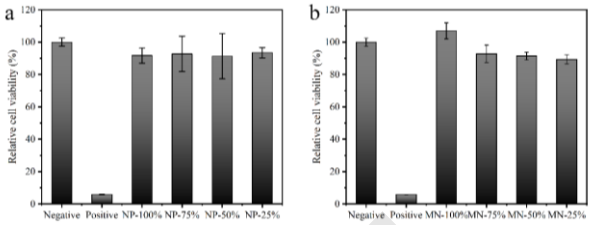

Fig. 19 MTT study: (a) NP-PEG$_{114}$-*b*-PAAPBA$_{291}$; (b) blank MN zk-7.5%

3.8 *In vivo* insulin release assay

The microneedle patches were applied to a type 1 diabetes rat model. The study started with the beginning of fasting at 0 h, and each group of rats was treated at 3 h. Blood glucose concentrations were measured every hour to assess their glycemic control performance over time. Treatment groups included a healthy group (Health), microneedle group MN-va-7.5%-1 (0.044 IU insulin/g body weight), microneedle group MN-va-7.5%-2 (0.088 IU insulin/g body weight), subcutaneous injection of insulin group SC-1 (0.088 IU insulin/g body weight), a control group injected with PBS (PBS), and a microneedle group loaded with insulin MN-va-ins (0.088 IU insulin/g body weight). Figure 21 shows the blood glucose concentration curves over time for the six different treatment groups of rats. As the entire process involved fasting, all groups of rats experienced a decrease in blood glucose, with the PBS control group showing consistently high blood glucose levels, indicating the successful construction of the model. The Health group of rats initially maintained normal blood glucose levels but experienced hypoglycemia due to hunger around 6 h. However, the SC-1 group of rats developed severe hypoglycemic symptoms at the 6th hour and eventually died within 9-10 h, indicating a risk of serious hypoglycemia caused by subcutaneous insulin injection. For the microneedle groups, the MN-va-ins group of rats maintained normal blood glucose levels from 4.5 h to 7 h and then returned to high blood glucose levels, indicating limited glycemic control effectiveness of the microneedle directly loaded with insulin. The blood glucose concentration of the MN-va-7.5%-1 group of rats remained normal for about 2 h, indicating limited glycemic control effectiveness. However, the blood glucose concentration of the MN-va-7.5%-2 group of rats was maintained within the normal range from 4 hours to 11 h, indicating that this microneedle could effectively maintain blood glucose levels in rats at normal levels for more than 7 h and had good glycemic control effectiveness.

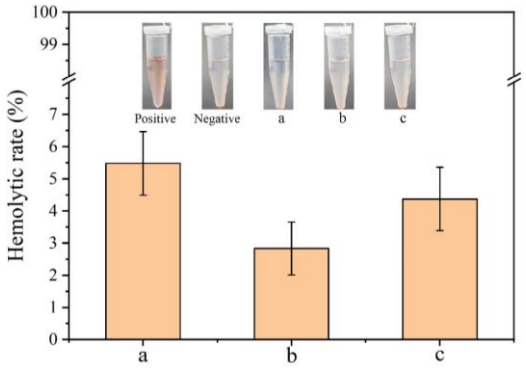

Fig. 20 Hemolysis experiment images and hemolysis rate of each sample, (a) NP-PEG$_{114}$-*b*-PAAPBA$_{117}$, (b) NP-PEG$_{114}$-*b*-PAAPBA$_{291}$, (c) NP-PEG$_{114}$-*b*-PAAPBA$_{324}$

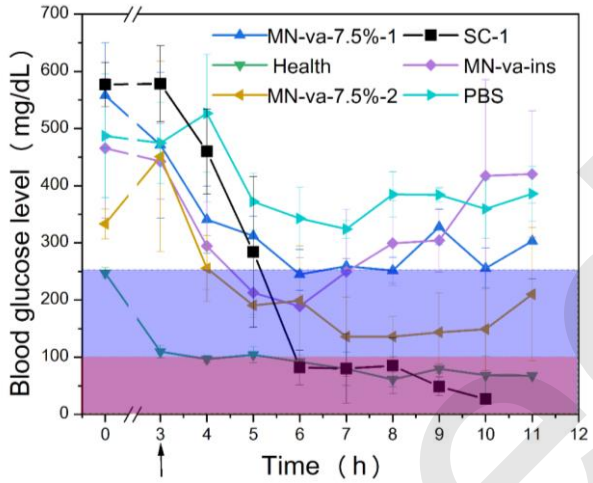

Fig. 21 Plasma glucose levels after administration of insulin-loaded MN patches. Animal model: SD rats with type I diabetes (n=4)

4. Conclusions

The PEG-DDMAT RAFT reagent was successfully synthesized and used to synthesize PEG-*b*-PAAPBA block copolymers with seven different chain lengths, characterized by FTIR and ^{1}H NMR. Four glucose-responsive particles, NP-PEG$_{114}$-*b*-AAPBA$_n$, and their corresponding insulin-loaded particles, ins-PEG$_{114}$-*b*-PAAPBA$_n$, were prepared using self-assembly methods by changing the hydrophilic-hydrophobic interaction of the polymer at different pH values. The glucose responsiveness of the particles was demonstrated by changes in particle size at different glucose concentrations and insulin release *in vitro*. Glucose-responsive microneedle patches were then produced using centrifugation and vacuum methods, and their morphology was characterized by SEM. The mechanical strength of the microneedles was proven to be sufficient for skin penetration using a universal testing machine and mouse skin puncture experiments. Safety tests, including hemolysis assays and MTT cytotoxicity assays, were conducted on the glucose-responsive microneedle patches, and *in vivo* experiments on rats showed that they could control blood glucose levels for over 7 h. The study found that the glucose responsiveness of the particles was affected mainly by the ratio of the PEG block to the AAPBA block. Stable hollow particles were formed when the PEG repeat unit number was 114 and the AAPBA repeat unit number was above 50 at a final pH of 7.4 during particle preparation. The drug loading efficiency of the selected insulin-loaded particle, ins-PEG$_{114}$-*b*-PAAPBA$_{291}$, was 61.2%. With increasing AAPBA content, the particles exhibited more sensitive glucose responsiveness. Ins-PEG$_{114}$-*b*-PAAPBA$_{291}$ released 0.22 mg, 0.32 mg, and 0.46 mg of loaded insulin at glucose concentrations of 0, 100, and 400 mg/dL, respectively, within 7 h. The microneedle patch MN-va-7.5%-2, produced using 7.5 wt% HA in a vacuum environment of 0.07 MPa for 2 h, effectively controlled blood glucose levels in rats at a normal level for over 7 h.

Acknowledgments

Financial support from the Natural Science Foundation of Zhejiang Province (LHDMZ22H300003) and the Science and Technology Program of Zhejiang Province (2019C03063) is gratefully acknowledged.

Author contributions

Yichuan HONG designed and performed the research, wrote the original draft. Haojie YU supervised the porject and revised the paper. Li WANG revised the paper. Xiang CHEN Di SHEN and Yu WANG analyzed the data. Shuning REN and Yudi HUANG revised the manuscript. Jian YANG analyzed the data.

Conflict of interest

Yichuan HONG, Haojie YU, Li WANG, Xiang CHEN, Di SHEN, Yu WANG, Shuning REN, Yudi HUANG, Jian YANG declare that they have no conflict of interest.

References

Mayer-Davis E J, Lawrence J M, Dabelea D, et al, 2017. Incidence trends of type 1 and type 2 diabetes among youths,

2002-2012. *The New England Journal of Medicine*, 376(15): 1419-1429. https://doi.org/10.1056/NEJMoa1610187.

Chan J C N, Lim L L, Wareham N J, et al., 2020. The lancet commission on diabetes: using data to transform diabetes care and patient lives. *The Lancet*, 396(10267): 2019-2082. https://doi.org/10.1016/s0140-6736(20)32374-6

American Diabetes Association, 2018. 2. Classification and diagnosis of diabetes: standards of medical care in diabetes-2018. *Diabetes Care*, 41(Suppl 1): S13-S27. https://doi.org/10.2337/dc18-S002

Meng F, Hasan A, Mahdi Nejadi Babadaei M, et al., 2020. Polymeric-based microneedle arrays as potential platforms in the development of drugs delivery systems. *Journal of Advanced Research*, 26: 137-147. https://doi.org/10.1016/j.jare.2020.07.017

Chen S, Miyazaki T, Itoh M, et al., 2020. Temperature-stable boronate gel-based microneedle technology for self-regulated insulin delivery. *ACS Applied Polymer Materials*, 2: 2781-2790. https://doi.org/10.1021/acsapm.0c00341

Li L, Jiang G, Du X, et al., 2015. Preparation of glucose-responsive and fluorescent micelles *via* a combination of RAFT polymerization and chemoenzymatic transesterification for controlled release of insulin. *RSC Advances*, 5(92): 75766-75772. https://doi.org/10.1039/c5ra15281j

Wu J Z, Williams G R, Li H Y, et al., 2017. Glucose- and temperature-sensitive nanoparticles for insulin delivery. *International Journal of Nanomedicine*, 12: 4037-4057. https://doi.org/10.2147/IJN.S132984

Tong Z, Zhou J, Zhong J, et al., 2018. Glucose- and H_2O_2-responsive polymeric vesicles integrated with microneedle patches for glucose-sensitive transcutaneous delivery of insulin in diabetic rats. *ACS Applied Materials & Interfaces*, 10(23): 20014-20024. https://doi.org/10.1021/acsami.8b04484

Senemoğlu Y, Hazer B, Arslan H, et al., 2022. Synthesis and physicochemical characterization of PMMA and PNIPAM based block copolymers by using PEG based macro RAFT agents. *Journal of Chemical Sciences*, 134(2): 49. https://doi.org/10.1007/s12039-022-02047-z

Zhou H, Liu C, Gao C, et al., 2016. Polymerization-induced self-assembly of block copolymer through dispersion RAFT polymerization in ionic liquid. *Journal of Polymer Science Part A: Polymer Chemistry*, 54(11): 1517-1525. https://doi.org/ 10.1002/pola.28002

Wang J, Yu J, Zhang Y, et al., 2019. Charge-switchable polymeric complex for glucose-responsive insulin delivery in mice and pigs. *Science Advances*, 5(7): eaaw4357. https://doi.org/10.1126/sciadv.aaw4357

Yu J, Wang J, Zhang Y, et al., 2020. Glucose-responsive insulin patch for the regulation of blood glucose in mice and minipigs. *Nature Biomedical Engineering*, 4(5): 499-506. https://doi.org/10.1038/s41551-019-0508-y

Shen D, Yu H, Wang L, et al., 2020. Recent progress in design and preparation of glucose-responsive insulin delivery systems. *Journal of Controlled Release*, 321: 236-258. https://doi.org/10.1016/j.jconrel.2020.02.014

Chen X, Yu H, Wang L, et al., 2021. Microneedle patch prepared from a hydrogel by a mild method for insulin delivery. *ChemNanoMat*, 7(11): 1230-1240. https://doi.org/10.1002/cnma.202100288

中文概要

题　目：聚乙二醇-*b*-聚丙烯酰胺基苯硼酸葡萄糖响应粒子及其透明质酸微针贴片的制备与性能研究

作　者：洪溢川[1]，俞豪杰[1,2]，王立[1,2]，陈翔[1]，沈迪[1]，任书宁[1]，黄宇笛[1]，杨健[1]

机　构：[1]浙江大学，化学工程联合国家重点实验室，化学工程与生物工程学院，中国杭州，310058；[2]浙江-俄罗斯光电磁功能材料联合实验室，中国杭州，310058

目　的：微针给药具有高效、方便、无痛等特点，有望用于透皮递送胰岛素治疗糖尿病。本文旨在制备糖敏响应负载胰岛素粒子，然后与透明质酸混合制备糖敏微针贴，研究其糖敏响应性能和对糖尿病大鼠的血糖控制性能。

创新点：1. 通过嵌段共聚物的亲疏水自组装制备了葡萄糖响应粒子并负载了胰岛素；2. 制备了苯硼酸基糖敏微针贴，具有较好的血糖控制性能。

方　法：1. 通过 RAFT 反应制备了不同链长的 PEG-*b*-PAAPBA 嵌段共聚物（图 4）；2. 通过嵌段共聚物在不同 pH 值下的亲疏水相互作用，自组装制备了葡萄糖响应粒子 NP-PEG114-*b*-AAPBAn 并负载了胰岛素（图 7）；3. 用 NP-PEG114-*b*-AAPBAn 负载胰岛素粒子和透明质酸制备了糖敏微针贴，通过动物实验验证了所得糖敏微针贴片具有较好的血糖控制性能（图 15 和图 21）。

结　论：1. 合成了不同链长的 PEG-*b*-PAAPBA 嵌段共聚物，通过自组装方法制备了葡萄糖响应粒子 NP-PEG114-*b*-AAPBAn 并负载了胰岛素；2. 用 NP-PEG114-*b*-AAPBAn 负载胰岛素粒子和透明质酸制备了糖敏微针贴；3. 所得糖敏微针贴片可以将糖尿病大鼠的血糖控制在正常水平超过 7 小时。

关键词：糖尿病；透明质酸；苯硼酸；糖敏水凝胶；微针